Journal of Physics D: Applied Physics

PAPER • **OPEN ACCESS**

Large electrocaloric effect and energy storage performance of site-engineered lead-free $Ba_{1-x}(Bi_{0.5}Li_{0.5})_xTiO_3$ ferroelectric oxides

To cite this article: Subhajit Pal *et al* 2021 *J. Phys. D: Appl. Phys.* **54** 045302

OPEN ACCESS
IOP Publishing
Journal of Physics D: Applied Physics
J. Phys. D: Appl. Phys. **54** (2021) 045302 (9pp)
https://doi.org/10.1088/1361-6463/abbeb4

Large electrocaloric effect and energy storage performance of site-engineered lead-free $Ba_{1-x}(Bi_{0.5}Li_{0.5})_xTiO_3$ ferroelectric oxides

Subhajit Pal[1], Pranab Parimal Biswas[1], Martando Rath[1,2], M S Ramachandra Rao[1,2], Muralidhar Miryala[3], Masato Murakami[3] and Pattukkannu Murugavel[1]

[1] Department of Physics, Indian Institute of Technology Madras, Chennai 600036, India
[2] Department of Physics, Nano Functional Materials Technology Centre and Materials Science Research Centre, Indian Institute of Technology Madras, Chennai 600036, India
[3] Graduate School of Science and Engineering, Superconducting Materials Laboratory, Shibaura Institute of Technology, 3-7-5 Toyosu, Koto-ku, Tokyo 135-8548, Japan

E-mail: muruga@iitm.ac.in

Received 19 July 2020, revised 25 September 2020
Accepted for publication 6 October 2020
Published 9 November 2020

Abstract

Environment-friendly solid-state cooling technology necessitates the search for energy-efficient electrocaloric (EC) materials. In this regard, the EC effect and energy storage performance have been investigated on a site-engineered lead-free $Ba_{1-x}(Bi_{0.5}Li_{0.5})_xTiO_3$ ($x = 0.0$, 0.10, 0.125, 0.15 and 0.175) system from the perspective of its enhanced characteristic parameters. The ferroelectric and dielectric studies reveal the tunable polarization and Curie temperature as a function of composition. The EC measurements on these samples display superior EC parameters compared to the values reported for other polycrystalline ferroelectric systems. The observed EC parameters for the $x = 0.10$ sample, such as the change in entropy (ΔS), adiabatic temperature change (ΔT) and EC coefficient are 2.63 J kg^{-1} K, 2.03 K and 0.68 K mm^{-1} kV, respectively. Notably, the $x = 0.15$ sample displays near room-temperature (307 K) EC response with $\Delta T \geq 0.30$ K over a broad 24 K temperature range. In addition, the energy storage performance studies elucidate that the $Ba_{1-x}(Bi_{0.5}Li_{0.5})_xTiO_3$ compound with $x = 0.175$ displays large energy storage efficiency (96.7%) with 144 mJ cm^{-3} as the storage density. The tunable EC characteristics and high energy storage efficiency demonstrated in this work illustrate the application potential of site-engineered $BaTiO_3$ samples in efficient cooling and storage devices.

Supplementary material for this article is available online

Keywords: ferroelectric, polarization, pyroelectric, electrocaloric effect, energy storage device

(Some figures may appear in colour only in the online journal)

1. Introduction

In recent years, the electrocaloric (EC) effect has drawn more research attention due to its energy-efficient capabilities in eco-friendly solid-state cooling devices compared to vapor-compression refrigerators [1–3]. The EC effect in the pyroelectric system and the associated adiabatic temperature

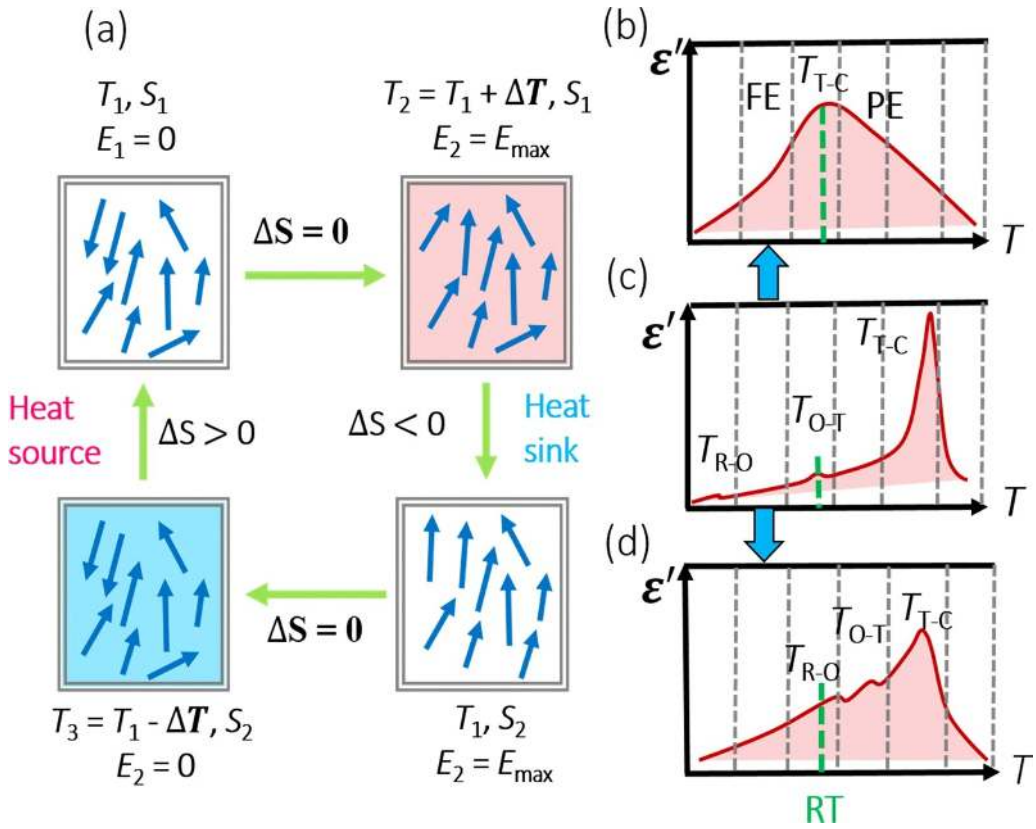

Figure 1. Schematic of (a) the working principle of EC effect, (b) coexistence of various phase transitions at RT in modified BTO, (c) various phase transitions in BTO and (d) various phase transitions observed above RT in modified BTO.

change (ΔT) are the consequence of the dipole arrangements facilitated by the applied electric field [4]. During the EC cyclic process, schematically shown in figure 1(a), the dipole orientation under electric field (E) lowers the entropy of the system by transferring the heat to the sink. Subsequently, the material is allowed to cool through the adiabatic process by the reorientation of dipoles upon withdrawal of the field and finally reaches the initial state by absorbing heat from the surrounding temperature [4, 5]. Importantly, the change in entropy of the system is correlated to the strength and dynamics of polarization [6]. Significant polarization change observed near ferroelectric-paraelectric phase transition temperature (T_C) generally yields a large EC response [2]. Besides, studies have also been carried out to achieve large EC response in ferroelectric oxides through geometrical optimization, multi-phase coexistence, combining positive and negative caloric responses, and introducing an extra degree of freedom such as mechanical stress/pressure [7]. Among all these approaches, the multi-phase coexistence near T_C achieved via lattice-site engineering in the $BaTiO_3$ (BTO) system, such as $(Ba_{0.87}Ca_{0.13})(Ti_{0.87}Hf_{0.13})O_3$ and (1-x)$Ba(Ti_{0.89}Sn_{0.11})O_3$-$x(Ba_{0.7}Ca_{0.3})TiO_3$ resulted in large EC effect [8, 9]. Although the near room-temperature (RT) EC effect is reported in a few systems, most of the large EC responses are perceived either far above or below RT [8–12].

Generally, studies have been done to tune the ferroelectric T_C towards RT through lattice-site, defect, and strain engineering [8, 13, 14]. Note that BTO exhibits rhombohedral to orthorhombic (R-O), orthorhombic to tetragonal (O-T) and tetragonal to cubic (T_C) at 183, 283 and 397 K, respectively, as schematically shown in figure 1(c) [15, 16]. So far, in the modified BTO system, effort has been made to enhance the EC parameters by bringing these phase transitions above RT (shown in the schematic figure 1(d)) [9]. This can be achieved by changing the energy landscape upon doping. For example, in the (1-x)$Ba(Ti_{0.89}Sn_{0.11})O_3$-$x(Ba_{0.7}Ca_{0.3})TiO_3$ and $Ba(Ti_{1-x}Sn_x)O_3$ systems, the R-O and O-T transitions are brought above RT, but without phase coexistence at a particular temperature [17, 18]. However, the ferroelectric system with coexisting phases at or near RT, as displayed in schematic figure 1(b), could be a better candidate for EC applications. For example, $(Ba_{0.87}Ca_{0.13})(Ti_{0.87}Hf_{0.13})O_3$ having a flattened energy landscape due to the phase coexistence near RT shows large EC effect [8].

Apart from tuning the phase coexistence, the lattice-site engineering in the BTO system may also offer another fascinating physical property called relaxor, which is associated with a diffuse phase transition over a broad temperature range [15, 19]. Besides showing the EC effect, the relaxor ferroelectric system can be used for high energy storage applications at RT, due to its slim hysteresis, large maximum polarization (P_{max}) and small remnant polarization (P_r). For example, the temperature-dependent dielectric and ferroelectric studies on the (1-x)(0.65$BaTiO_3$-0.35$Bi_{0.5}Na_{0.5}TiO_3$)-$xSr(Sc_{0.5}Nb_{0.5})O_3$ relaxor ferroelectric illustrate a large variation of the energy storage performance, which is mainly

explained from the domain structure of the system [20]. The temperature-dependent ferroelectric features observed in the (1-x)(0.65$BaTiO_3$-0.35$Bi_{0.5}Na_{0.5}TiO_3$)-$xSr(Sc_{0.5}Nb_{0.5})O_3$ system show a similar trend with compositional-dependent features observed in $Ba_{1-x}(Bi_{0.5}Li_{0.5})_xTiO_3$ (BBLT) systems. Hence, the BBLT systems could be a suitable candidate to achieve high energy storage performance.

In view of this, studies have been carried out to investigate the EC effect and energy storage capacity of the modified BTO samples, which are reported to show the coexistence of orthorhombic and tetragonal phases along with near RT T_C [15]. Notably, for better EC response, it is imperative to sustain the polarization value while tuning the T_C of the ferroelectric system. In this context, the earlier studies on Bi and Li co-doped BTO samples revealing the tunable characteristic of T_C with enhanced polarization, illustrate its potential to yield a large EC effect near RT [15, 21]. In this work, the composition-dependent EC effect and energy storage performance are investigated on the site-engineered BBLT samples. The results demonstrate a large and near RT EC effect along with giant energy storage efficiency.

2. Experimental details

$Ba_{1-x}(Bi_{0.5}Li_{0.5})_xTiO_3$ (x = 0.0, 0.1, 0.125, 0.15 and 0.175) powders with different concentrations were prepared by a solid-state reaction route using stoichiometric mixtures of analytical reagent-grade $BaCO_3$ (99.9%), Bi_2O_3 (99.9%), Li_2CO_3 (99.9%) and TiO_2 (99.9%) powders. The mixed oxide powders were calcined by following the procedure reported elsewhere [15, 21]. The calcined powder was mixed with 6 wt.% polyvinyl alcohol and pressed into 8 and 12 mm diameter green pellets using a uniaxial press. The BBLT pellets were sintered for 2 h at 1300 °C for x = 0.0, 1050 °C for x = 0.10 and 1000 °C for x = 0.125, 0.15 and 0.175 samples. The decrease in sintering temperature is in accordance with the increase in volatile Bi and Li concentrations. The density of the sintered pellets was found to be ∼96% of the theoretical density.

The x-ray diffraction (XRD) (Rigaku SmartLab) experiments were carried out using Cu Kα radiation to study the structural information. The polarization measurements were carried out by employing a Radiant Technology (USA RT6000S) ferroelectric loop tracer. The temperature-dependent dielectric constant was measured at various frequencies using a Nova Control (Alpha-A) high-performance frequency analyzer. The specific heat of the BBLT sample was carried out by a Quantum Design Physical Property Measurement System (DynaCool-D212). For pyroelectric measurements, the Ag electrodes were coated on both sides of the pellets. The pyroelectric measurements were carried out inside a cryostat (Advanced Research System) by employing a Keithley electrometer (6517B) as a current source. The microstructures of the sintered pellets were recorded by field-emission scanning electron microscopy (FE-SEM, JEOL, JSM-7610F) after depositing gold conducting layer on the pellets by sputtering.

3. Results and discussion

The consolidated results of the basic characteristics of the BBLT (x = 0.0, 0.10, 0.125, 0.15 and 0.175) samples are shown in figure S1 (supplementary material, available online at http://stacks.iop.org/JPhysD/54/045302/mmedia), where the respective XRD patterns, polarization (P) versus E measured at 4 Hz, and composition-dependent P_r are plotted. The structural analysis reported earlier on the BBLT system revealed the coexistence of tetragonal and orthorhombic phases [15]. The reduction in tetragonality factor (c/a) for higher doping concentrations is evident from the merging of the (002) and (200) diffraction peaks shown in the enlarged version of the XRD patterns in figure S1(b) [21]. The P_r value shows maximum (9.76 μC cm^{-2}) for the x = 0.10 sample, followed by a decreasing trend with composition. Importantly, the x = 0.15 sample displays a nearly equivalent P_r value to the parent BTO sample. However, the x = 0.175 sample shows a thin hysteresis loop with nearly vanishing P_r. This could be due to the system moving towards cubic symmetry, as revealed by the XRD pattern.

To understand the dielectric behavior and the ferroelectric phase transitions, the temperature-dependent dielectric permittivity of all compositions is measured at 10 kHz, and the corresponding real part of the permittivities (ε') is plotted in the insets of figures 2(a)–(d). The temperature variation of ε' reveals that the T_C of the modified BTO samples shows a decrease in value from that of the parent BTO. In contrast, the earlier report on the BBLT samples for $0 < x < 0.1$ shows a systemic increase in T_C with composition [22]. Note that the physical properties of the sample could vary with sintering conditions. A report on the $Ba_{0.98}(Bi, Li)_{0.02}TiO_3$ system revealed that the T_C decreases with a reduction in sintering temperature [23]. Hence, the change in T_C observed in BBLT is correlated to the variations in sintering temperatures. To gain further insight into the dielectric properties, the dielectric data are analyzed using the modified Curie–Weiss law, $1/\varepsilon'$—$1/\varepsilon'_{max} = [(T—T'_{max})/C]^{\gamma}$, where ε'_{max} is the value of ε' at T'_{max}, C is the Curie constant, and γ is the diffusivity parameter [15, 19]. Accordingly, the $1/\varepsilon'$—$1/\varepsilon'_{max}$ is plotted against temperature for the x = 0.10, 0.125, 0.15 and 0.175 samples in figures 2(a)–(d), respectively. The characteristic parameters T'_{max} and γ are extracted by fitting the plots with the modified Curie–Weiss equation. The extracted T'_{max} values are 381, 352, 325 and 388 K for the x = 0.10, 0.125, 0.15 and 0.175 samples, respectively. It is observed that the x = 0.175 sample shows two dielectric anomalies at 283 and 388 K. The possible origin of the dielectric anomalies for x = 0.175 can be understood from the temperature-dependent plots of ε' and tanδ at various frequencies, as shown in figure S2. The anomaly near 283 K shows the frequency dispersive features, whereas the anomaly at 388 K shows nearly frequency-independent characteristics. These two anomalies could be correlated to relaxor and phase transition-like anomalies assisted by local charge disorder and oxygen vacancy related defects, respectively [15, 24, 25]. It is worth mentioning that the x = 0.15 composition shows T_C near RT and, at the same time, retaining the P_r (6.1 μC cm^{-2}), equivalent to the parent BTO sample (5.5 μC cm^{-2}). Interestingly,

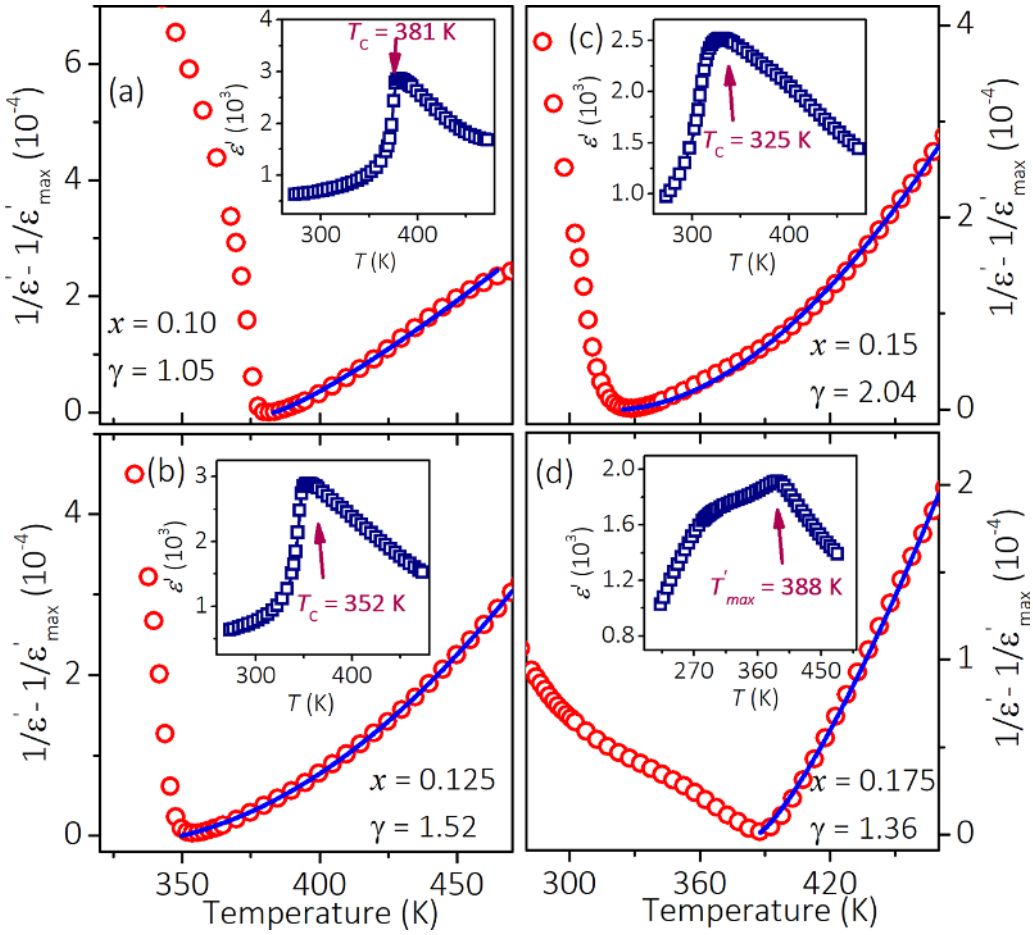

Figure 2. Modified Curie–Weiss plots of (a) $x = 0.10$, (b) $x = 0.125$, (c) $x = 0.15$ and (d) $x = 0.175$ BBLT samples at 10 kHz. Insets show respective ε' plots.

all other compositions excluding $x = 0.10$ are identified to be the relaxor in nature based on their γ values, where γ is expected to be well above 1 and preferably around 2 for the system to be a relaxor [26].

To investigate the EC response in BBLT samples, temperature-dependent pyroelectric current measurements are performed to get the corresponding polarization values. Before the measurements, the samples are heated up to 390 K, which is well above the T_C of the BBLT samples, and cooled down to suitable temperatures at 5 K min^{-1} under the poling field. The pyroelectric current is then measured during the warming cycle after removing the poling field. The measurements are repeated at various poling fields from 5–30 kV cm^{-1}. The measured pyroelectric current (i) is used to extract the P values using the $P = \frac{1}{A\beta}\int i dT$ relation, where A, β, and dT are the surface area, heating rate, and change in temperature of the sample, respectively [27]. The obtained P is plotted against temperature at 5, 10, 15, 20 and 30 kV cm^{-1} poling fields for $x = 0.10$, 0.125, 0.15 and 0.175 in figures 3(a)–(d), respectively. The P_{max} values obtained after subjecting 30 kV cm^{-1} poling fields for $x = 0.10$, 0.125, 0.15 and 0.175 samples at RT (300 K) are 9.46, 7.28, 4.10 and 0.70 μC cm^{-2}, respectively.

The composition-dependent P values extracted at RT for the BBLT samples are similar to the experimental values observed from the P-E measurements shown in figure S1(d). These features illustrate the fact that the pyroelectric and P-E measurements are complementary techniques to get the P values. Also, the temperature-dependent P-E hysteresis loops for all the BBLT samples are measured at RT, and they are shown in figure S3. The systematic variations in temperature-dependent polarization responses illustrate that the pyroelectric current response obtained from the pyroelectric measurements mainly originated from the intrinsic pyroelectric response rather than ion migration and defects. All samples except $x = 0.175$ reveal typical pyroelectric current behavior of the ferroelectric samples with a drop in P near the vicinity of T_C. On the other hand, the $x = 0.175$ sample shows a monotonous decrease in P throughout the measurement temperature range. The large decrease in polarization for $x = 0.175$ with respect to the other BBLT samples could be correlated to the cubic-like crystal structure of the sample, which is evident from the singlet nature of the (002)/(200) Bragg's peaks, as shown in figure S1(b).

The EC response of the BBLT system can be extracted from the measured pyroelectric current using the thermodynamic Maxwell's relation $\left(\partial T/\partial E\right)_T = -\frac{T}{C_P \rho}\left(\partial P/\partial T\right)_E$ [28–30], where $\frac{dP}{dT} =$ is the pyroelectric coefficient and ρ and C_P are

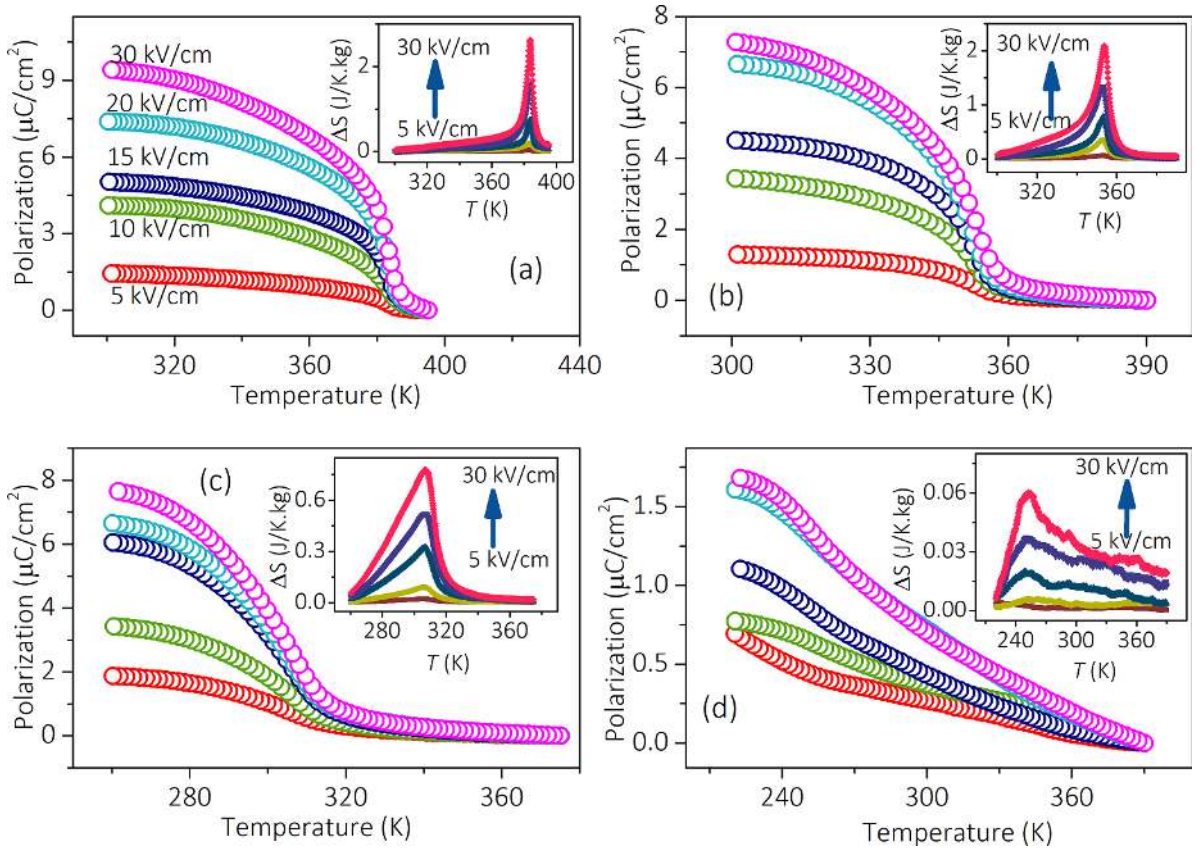

Figure 3. Temperature-dependent P measurements for (a) $x = 0.10$, (b) $x = 0.125$, (c) $x = 0.15$ and (d) $x = 0.175$ BBLT samples at various poling fields. Insets show respective ΔS plots.

the mass density and heat capacity, respectively. Generally, EC response is determined either from direct heat flow measurements under the electric field or from indirectly obtained α value using the P-E loop measurements [31, 32]. Alternatively, the EC response can also be calculated from the direct determination of α using the relation $i(T) = A\frac{\partial P}{\partial t} = A\frac{\partial P}{\partial T}\frac{\partial T}{\partial t} = A\beta$ [28, 29, 33]. In ferroelectric systems, the obtained α value is found to be in good agreement with the value calculated from indirect measurements [28, 29]. Hence, the change in entropy in the system can be calculated using the thermodynamic Maxwell's equation $\left(\partial P/\partial T\right)_E = \left(\partial S/\partial E\right)_T$, and the resultant isothermal entropy change (ΔS) can be expressed as, $\Delta S = -\frac{1}{A\beta\rho} i(T)\,\Delta E$ [32]. Here, $\Delta E = E_1 - E_2$ is the difference in initial (E_1) and final (E_2) poling fields, respectively. The β is 5 K min^{-1} during the heating cycle. The calculated ΔS for different compositions is plotted in the insets of figures 3(a)–(d). The plots display a sharp rise in ΔS with maximum values of 2.63 and 2.1 J kg^{-1} K for the $x = 0.10$ and 0.125 compositions at 382 and 351 K, respectively. On the other hand, for the $x = 0.15$ sample, the ΔS shows a linear increment with temperature and reaches a maximum value of 0.78 J kg^{-1} K at 307 K. The maximum ΔS observed at 307 K instead of its T_C (325 K) for the $x = 0.15$ sample, could be correlated to the electric field-induced effect on the transition temperature in relaxor dielectrics [34]. The $x = 0.175$ sample displays almost negligible ΔS, which is expected based on its polarization feature.

In addition, ΔT values for BBLT samples are calculated using the equation $\Delta T = -\frac{T}{A\beta C_P \rho} i(T)\,\Delta E$ [28]. To obtain ΔT, the C_P value for each sample is taken to be the same throughout the measurement temperatures range, while its actual variation with temperature is shown in the insets of figures 4(a)–(c) for the $x = 0.10$, 0.125 and 0.15 samples, respectively [8]. The C_P values at T_C are used for ΔT evaluation and they are 0.509, 0.485 and 0.471 J g^{-1} K for the $x = 0.10$, 0.125 and 0.15 samples, respectively. The ΔT calculated at different poling fields by keeping the lower limit $E_1 = 0$ is plotted as a function of temperature in figures 4(a)–(c) at various E_2. Both ΔS and ΔT displayed similar temperature-dependent feature with compositions. The obtained ΔT displays the maximum of 2.03, 1.27 and 0.51 K values for the $x = 0.10$, 0.125 and 0.15 samples, respectively, at 30 kV cm^{-1}. Also, the obtained ΔT for $x = 0.175$ displayed in figure S4 exhibits negligible response in comparison to other BBLT samples. To illustrate the compositional variation of T_C and ΔT, the ΔT versus temperature plots at 30 kV cm^{-1} are displayed in figure 4(d). The histogram depicting the EC coefficients ($\Delta T/\Delta E = \Delta T/(E_2\text{-}E_1)$) calculated for different BBLT compositions is shown in the inset of figure 4(d), and the respective values are 0.68, 0.42 and 0.18 K mm^{-1} kV. For comparison, the histogram also

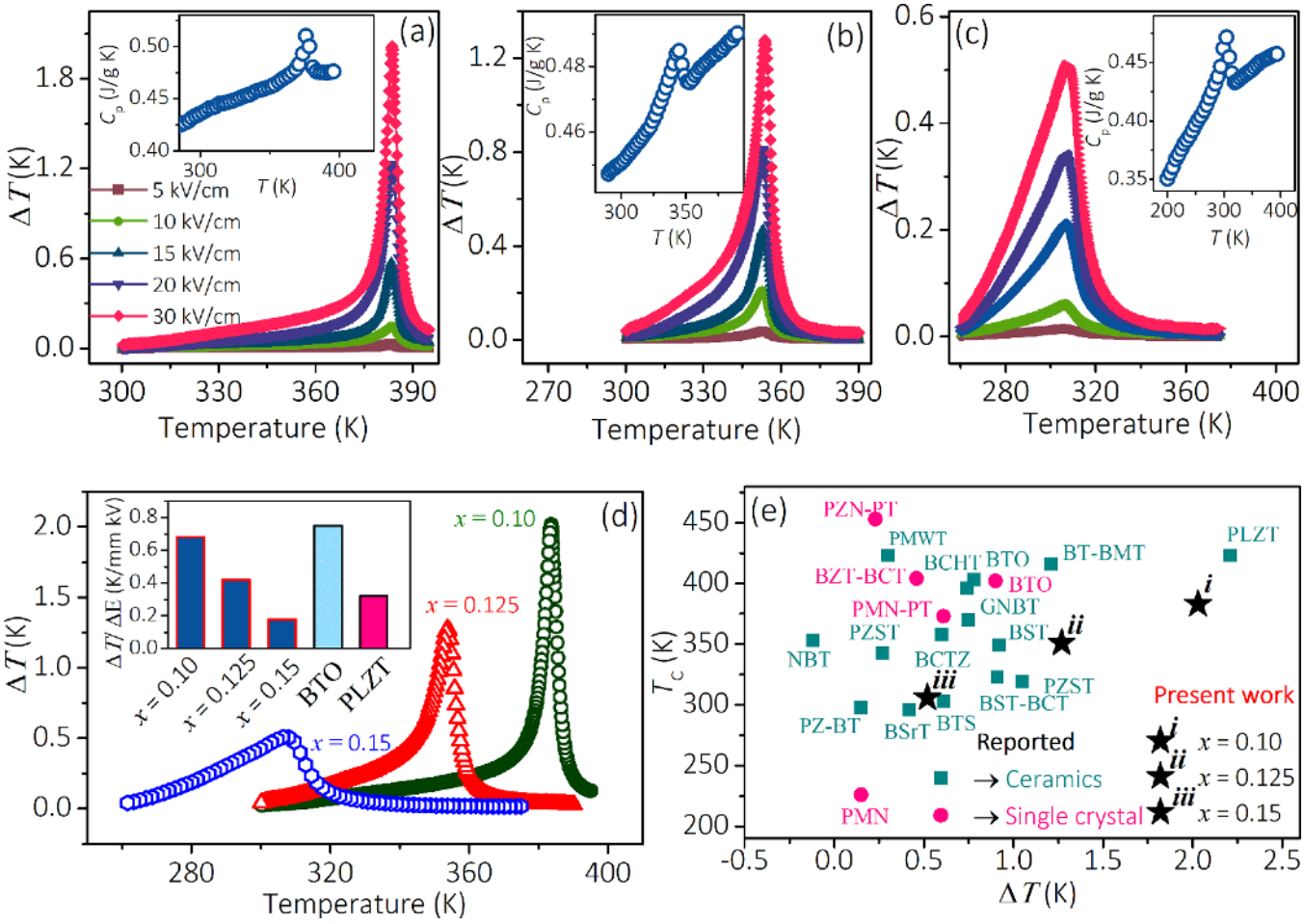

Figure 4. Temperature-dependent ΔT for (a) $x = 0.10$, (b) $x = 0.125$ and $x = 0.15$ BBLT samples measured at different poling fields. Respective insets display their temperature-dependent C_P. (d) ΔT plotted for $x = 0.10$, 0.125 and 0.15 at 30 kV cm^{-1}. Inset shows the histogram depicting the EC coefficient for the samples. (e) Summary of the reported values of ΔT and their corresponding T_C along with the results on BBLT samples.

shows the results of the single-crystalline BTO and polycrystalline PLZT samples. It is worth mentioning that the $x = 0.10$ sample displays the EC coefficient with a value close to the value reported (0.75 K mm^{-1} kV) for single-crystal BTO, and it is even higher than the few maximum reported ferroelectric systems [1, 35–38]. A summary of the literature data on the EC effect measured using the direct and indirect methods, such as T_C, maximum poling field (E_{max}), ΔT and $\Delta T/\Delta E$ are listed in table 1. The highest observed ΔT and their respective T_C of the reported compounds showing large EC effect are plotted in figure 4(e). From figure 4(e), it is clear that the BBLT sample with $x = 0.10$ exhibits one of the best ΔT values (next to PLZT) reported so far in the literature [39]. Also, the $x = 0.15$ sample shows $\Delta T \geq 0.30$ K over a broad range of temperature (24 K), i.e. from 289–313 K, which is also on the higher side among the reported values for other ferroelectric systems [8].

The diffuseness parameter extracted on the BBLT compositions suggests the existence of possible relaxor characteristics of the samples. The ferroelectric systems and, in particular, the relaxor ferroelectrics are being actively considered as energy storage materials. The recoverable energy density of the ferroelectric capacitor during the charging and discharging process is expressed as $W_{rec} = \int_{P_r}^{P_{max}} E\, dP$ [48]. To investigate the energy storage characteristics of the BBLT samples, their full *P-E* loops recorded at 4 Hz are plotted in figures 5(a)–(e). The obtained W_{rec} for $x = 0.0$, 0.10, 0.125, 0.150 and 0.175 are 107, 56, 60, 79 and 144 mJ cm^{-3}, respectively. The respective energy storage efficiency (η) calculated from $= \frac{W_{rec}}{W} \times 100$ is 50.4, 23.0, 34.5, 44.2 and 96.7%, where W is the total energy density extracted from $W = \int_{0}^{P_{max}} E\, dP$ [48]. Compared to other compositions, the $x = 0.175$ exhibits superior energy storage performance both in terms of W_{rec} and η. Although the $x = 0.175$ sample shows remarkable 96.7% η, the moderate W_{rec} value observed in the system can be correlated to the presence of smaller-size nanodomains [20]. The possible ways to improve the energy storage density in a ferroelectric system are to increase the potential of the material to sustain the maximum applied electric field without undergoing breakdown and to maximize the difference between

Table 1. Comparison of the T_C, maximum poling field (E_{max}), ΔT, and $\Delta T/\Delta E$ reported on ceramic and single-crystalline ferroelectric systems along with the results on BBLT samples measured by indirect and direct methods.

Systems	T_C (K)	E_{max} (kV cm^{-1})	ΔT (K)	$\Delta T/\Delta E$ (K mm kV^{-1})	Method
$BaTiO_3$ (BTO)	403	55	0.78	0.142 [40]	Indirect
$0.98BaTiO_3$-$0.02BiMg_{0.5}Ti_{0.5}O_3$ (BT-BMT)	416	55	1.21	0.220 [40]	Indirect
$Ba_{0.85}Ca_{0.15}Ti_{0.90}Hf_{0.10}O_3$ (BCTH)	396	35	0.74	0.211 [41]	Indirect
$Ba_{0.94}Sm_{0.04}TiO_3$ (BST)	347	30	0.92	0.306 [42]	Indirect
$Ba_{0.65}Sr_{0.35}TiO_3$ (BSrT)	296	20	0.42	0.210 [43]	Indirect
$BaTi_{0.895}Sn_{0.105}O_3$ (BTS)	303	20	0.61	0.31 [3]	Indirect
$Ba_{0.91}Ca_{0.09}Zr_{0.14}Ti_{0.86}O_3$ (BCZT)	358	20	0.60	0.305 [44]	Direct
$Gd_{0.02}Na_{0.5}Bi_{0.48}TiO_3$ (GNBT)	370	90	0.75	0.083 [45]	Indirect
$0.9Ba(Ti_{0.89}Sn_{0.11})O_3$-$0.1(Ba_{0.7}Ca_{0.3})TiO_3$ (BTS-BCT)	323	15	0.91	0.35 [9]	Indirect/Direct
$Na_{0.5}Bi_{0.5}TiO_3$ (NBT)	353	50	−0.12	−0.024 [46]	Indirect
$Pb(Mg_{0.5}W_{0.5})_{0.5}Ti_{0.5}O_3$ (PMWT)	423	23	0.3	0.13 [35]	Indirect
$Pb(Zr_{0.43}Sn_{0.43}Ti_{0.14})O_3$ (PZST)	443	30	0.27	0.09 [47]	Indirect
$Pb(Zr_{0.455}Sn_{0.455}Ti_{0.09})O_3$ (PZST)	319	30	1.05	0.35 [47]	Indirect
$(PbZrO_3)_{0.71}$—$(BaTiO_3)_{0.29}$ (PZ-BT)	298	20	0.15	0.08 [47]	Indirect
$Pb_{0.89}La_{0.11}(Zr_{0.7}Ti_{0.3})_{0.9725}O_3$ (PLZT)	423	70	2.21	0.32 [39]	Indirect
BTO crystal	402	12	0.9	0.75 [1]	Indirect/Direct
$PbMg_{1/3}Nb_{2/3}O_3$ (PMN) crystal	226	15	0.15	0.10 [35]	Indirect
$0.75PbMg_{1/3}Nb_{2/3}O_3$–$0.25PbTiO_3$ (PMN-PT) crystal	373	1	0.61	0.61 [36]	Direct
$0.92PbZn_{1/3}Nb_{2/3}O_3$–$0.08PbTiO_3$ (PZN-PT) crystal	453	1.2	0.23	0.19 [37]	Direct
$0.45BaZr_{0.2}Ti_{0.8}O_3$–$0.55Ba_{0.7}Ca_{0.3}TiO_3$ (BZT-BCT) crystal	404	12	0.46	0.38 [38]	Indirect
BBLT ($x = 0.10$) Present work	383	30	2.03	0.68	Indirect
BBLT ($x = 0.125$) Present work	351	30	1.27	0.42	Indirect
BBLT ($x = 0.15$) Present work	307	30	0.51	0.18	Indirect

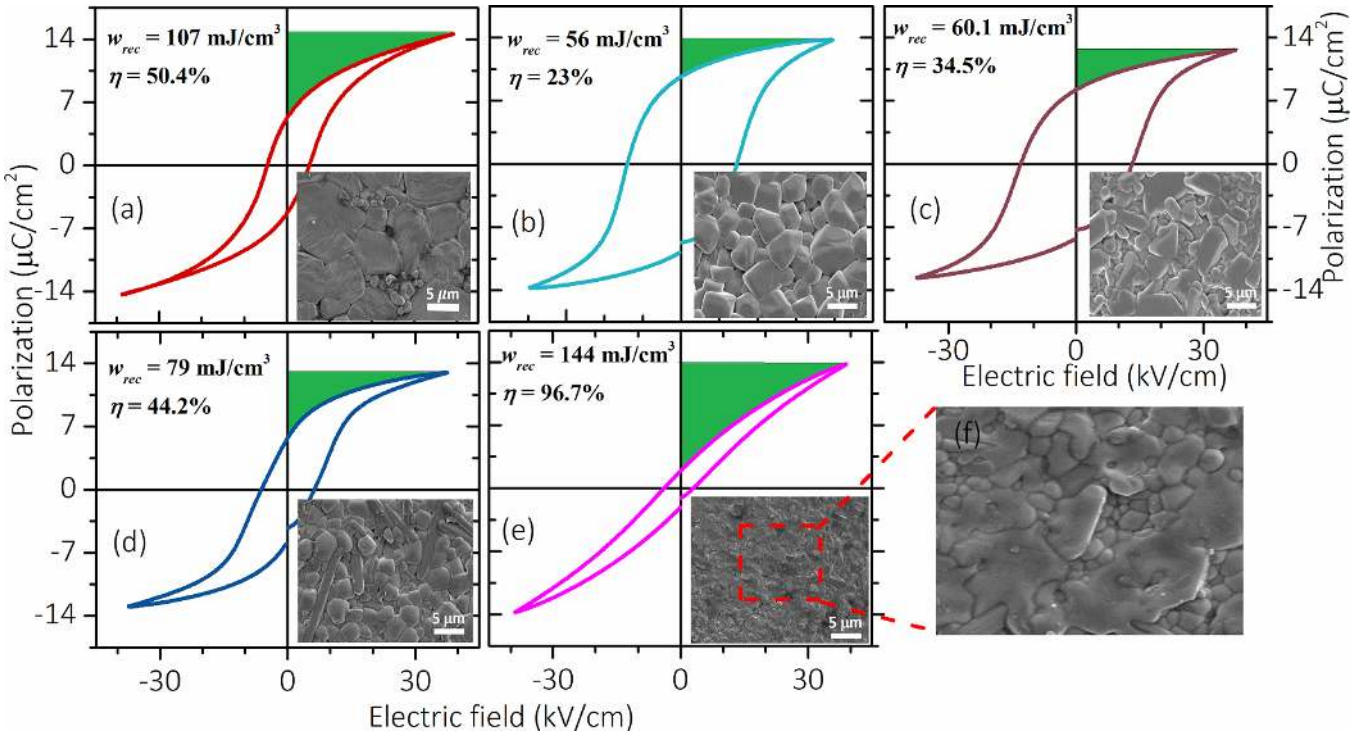

Figure 5. Polarization versus electric field plots for (a) $x = 0.0$, (b) $x = 0.10$, (c) $x = 0.125$, (d) $x = 0.15$ and (e) $x = 0.175$ compositions. Respective insets show the SEM microstructure of the samples. (f) Enlarged version of the SEM microstructure for the $x = 0.175$ sample.

P_{max} and P_r. In this context, the $x = 0.175$ composition displays the large difference between P_{max} and P_r due to its slim hysteresis loop characteristics with nearly vanishing P_r and hence shows better energy storage capacity. To get the microstructural correlation with the energy storage performance of the samples, the SEM microstructures obtained on the samples are shown in the insets of figure 5. The figures depict morphological change along with a decrease in porosity with composition. Notably, the $x = 0.175$ sample exhibits melted-like grain growth without any visible pore structure. The origin of the melted-like grain growth could be the eutectic phenomenon associated with higher doping concentration, which in turn facilitates lowering the melting point [49]. The melted-like grain structure exhibited by the $x = 0.175$ sample perhaps enhances its potential to sustain a higher electric field in comparison to other BBLT samples.

4. Conclusion

In summary, the structural, ferroelectric and dielectric studies on the site-engineered BTO systems elucidate the suitability of the material for large EC and energy storage devices. The composition-dependent EC response on the BBLT samples displays maximum of ΔS as 2.63, 2.1 and 0.78 J kg^{-1} K, and ΔT as 2.03, 1.27 and 0.51 K values for the $x = 0.10$, 0.125 and 0.15 samples poled under 30 kV cm^{-1}, respectively. Importantly, the $x = 0.10$ sample reveals superior EC coefficient of 0.68 K mm^{-1} kV, which is close to the value reported on single-crystal BTO (0.75 K mm^{-1} kV) and even higher compared to the values reported for other polycrystalline ferroelectric materials. Notably, $x = 0.15$ samples display near RT EC response with $\Delta T \geq 0.30$ K over a broad temperature range (289–313 K). In addition, the energy storage studies carried out on BBLT samples reveal that the $x = 0.175$ sample exhibits a remarkable 96.7% energy storage efficiency with 144 mJ cm^{-3} as recoverable energy density due to its suitable polarization characteristics. Overall, the large and tunable EC effect with high energy storage efficiency demonstrated on BBLT showcased the potential of this system for solid-state cooling and energy storage device applications.

Acknowledgments

The authors acknowledge the DST-FIST funding (Project No. SR/FST/PSII-038/2016) for the PPMS facility in the Department of Physics, IIT Madras, India. S P would like to thank the Japan Student Services Organization (JASSO) fellowship for carrying out some useful experiments in the Shibaura Institute of Technology (SIT) under the PhD innovative program, Tokyo, Japan.

ORCID iDs

Subhajit Pal https://orcid.org/0000-0002-5475-0988
Pranab Parimal Biswas https://orcid.org/0000-0002-4045-1194
M S Ramachandra Rao https://orcid.org/0000-0002-7505-5984
Muralidhar Miryala https://orcid.org/0000-0003-2205-0378
Masato Murakami https://orcid.org/0000-0002-6721-616X
Pattukkannu Murugavel https://orcid.org/0000-0002-4074-9118

References

[1] Moya X, Stern-Taulats E, Crossley S, Gonzalez-Alonso D, Kar-Narayan S, Planes A, Manosa L and Mathur N D 2013 *Adv. Mater.* **25** 1360
[2] Moya X, Kar-Narayan S and Mathur N D 2014 *Nat. Mater.* **13** 439
[3] Luo Z, Zhang D, Liu Y, Zhou D, Yao Y, Liu C, Dkhil B, Ren X and Lou X 2014 *Appl. Phys. Lett.* **105** 102904
[4] Scott J F 2011 *Annu. Rev. Mater. Res.* **41** 229
[5] Kumar R, Kumar A and Singh S 2019 *ACS Appl. Electron. Mater.* **1** 454
[6] Li X, Lu S G, Chen X Z, Gu H, Qian X and Zhang Q M 2013 *J. Mater. Chem.* C **1** 23
[7] Liu Y, Scott J F and Dkhil B 2016 *APL Mater.* **4** 064109
[8] Zhao L, Ke X, Zhou Z, Liao X, Li J, Wang Y, Wu M, Li T, Bai Y and Ren X 2019 *J. Mater. Chem.* C **7** 1353
[9] Zhao C, Yang J, Huang Y, Hao Y and Wu J 2019 *J. Mater. Chem.* A **7** 25526
[10] Zhang R, Peng S, Xiao D, Wang Y, Yang B, Zhu J, Yu P and Zhang W 1998 *Crys. Res. Technol.* **33** 827
[11] Lu S G, Rozic B, Zhang Q M, Kutnjak Z, Pirc R, Lin M, Li X and Gorny L 2010 *Appl. Phys. Lett.* **97** 202901
[12] Li X, Qian X, Lu S G, Cheng J, Fang Z and Zhang Q M 2011 *Appl. Phys. Lett.* **99** 052907
[13] Golovina I S, Falmbigl M, Hawley C J, Ruffino A J, Plokhikh A V, Karateev I A, Parker T C, Gutierrez-Perez A, Vasiliev A L and Spanier J E 2018 *Nanoscale* **10** 21798
[14] Liu Y, Infante I C, Lou X, Lupascu D C and Dkhil B 2014 *Appl. Phys. Lett.* **104** 012907
[15] Pal S, Swain A B, Sarath N V and Murugavel P 2020 *J. Phys.: Condens. Matter* **32** 365401
[16] Eisenschmidt C, Langhammer H T, Steinhausen R and Schmidt G 2012 *Ferroelectrics* **432** 103
[17] Zhao C *et al* 2018 *J. Am. Chem. Soc.* **140** 15252
[18] Gao J, Wang Y, Liu Y, Hu X, Ke X, Zhong L, He Y and Ren X 2017 *Sci. Rep.* **7** 40916
[19] Singh A, Moriyoshi C, Kuroiwa Y and Pandey D 2012 *Phys. Rev.* B **85** 064116
[20] Daia Z, Xiea J, Fana X, Dingb X, Liua W, Zhoua S and Ren X 2020 *Chem. Eng. J.* **397** 125520
[21] Pal S, Swain A B, Biswas P P, Murali D, Pal A, Nanda B R K and Murugavel P 2018 *Sci. Rep.* **8** 8005
[22] Rawat M and Yadav K L 2014 *Meter. Chem. Phys.* **148** 655
[23] Alkathy M S, Gayam R and James Raju K C 2016 *Ceram. Int.* **42** 15432
[24] Wang C C, Lei C M, Wang G J, Sun X H, Li T, Huang S G, Wang H and Li Y D 2013 *J. Appl. Phys.* **113** 094103
[25] Borkar H, Rao V, Dutta S, Barvat A, Pal P, Tomar M, Gupta V, Scott J F and Kumar A 2016 *J. Phys.: Condens. Matter* **28** 265901
[26] Bokov A A and Ye Z G 2006 *J. Mater. Sci.* **41** 31
[27] Sharp E J and Garn L E 1982 *J. Appl. Phys.* **53** 8980
[28] Kaddoussi H, Lahmar A, Gagou Y, Asbani B, Dellis J L, Cordoyiannis G, Allouche B, Khemakhem H, Kutnjak Z and El Marssi M 2016 *J. Alloys Compd.* **667** 198

[29] Asbani B, Dellis J L, Gagou Y, Kaddoussi H, Lahmar A, Amjoud M, Mezzane D, Kutnjak Z and El Marssi M 2015 *EPL* **111** 57008
[30] Lines M E and Glass A M 1977 *Principles and Applications of Ferroelectrics and Related Materials* (Oxford : Oxford University Press)
[31] Bai Y, Zheng G and Shi S 2010 *Appl. Phys. Lett.* **96** 192902
[32] Kumar R and Singh S 2018 *Sci. Rep.* **8** 3186
[33] Bsaibess E, Longuemart S, Soueidan M, Nsouli B and Sahraoui A H 2018 *J. Phys. D: Appl. Phys.* **51** 025306
[34] Fu D, Taniguchi H, Itoh M, Koshihara S, Yamamoto N and Mori S 2009 *Phys. Rev. Lett.* **103** 207601
[35] Valant M 2012 *Prog. Mater. Sci.* **57** 980
[36] Sebald G, Seveyrat L, Guyomar D, Lebrun L, Guiffard B and Pruvost S 2006 *J. Appl. Phys.* **100** 124112
[37] Valant M, Dunne L J, Axelsson A K, Alford N, Manos G, Perantie J, Hagberg J, Jantunen H and Dabkowski A 2010 *Phys. Rev.* B **81** 214110
[38] Singh G, Bhaumik I, Ganesamoorthy S, Bhatt R, Karnal A K, Tiwari V S and Gupta P K 2013 *Appl. Phys. Lett.* **102** 082902
[39] Lu B, Li P, Tang Z, Yao Y, Gao X, Kleemann W and Lu S G 2017 *Sci. Rep.* **7** 45335
[40] Li M D, Tang X G, Zeng S M, Liu Q X, Jiang Y P and Li W H 2018 *J. Alloys Compd.* **747** 1053
[41] Wang X, Wu J, Dkhil B, Zhao C, Li T, Lia W and Lou X 2017 *RSC Adv.* **7** 5813
[42] Han F, Bai Y, Qiao L J and Guob D A 2016 *J. Mater. Chem.* C **4** 1842
[43] Bai Y, Han X, Ding K and Qiao L J 2013 *Appl. Phys. Lett.* **103** 162902
[44] Wang J, Yang T, Chen S, Li G, Zhang Q and Yao X 2013 *J. Alloys Compd.* **550** 561
[45] Zannen M, Lahmar A, Kutnjak Z, Belhadi J, Khemakhem H and El Marssi M 2017 *Solid State Sci.* **66** 31
[46] Bai Y, Zheng G P and Shi S Q 2011 *Mater. Res. Bull.* **46** 1866
[47] Thacher P D 1968 *J. Appl. Phys.* **39** 1996
[48] Swain A B, Subramanian V and Murugavel P 2018 *Ceram. Int.* **44** 6861
[49] Kumar R, Asokan K, Patnaik S and Birajda B 2016 *J. Alloys Compd.* **687** 197